

HouseCat6D - A Large-Scale Multi-Modal Category Level 6D Object Pose Dataset with Household Objects in Realistic Scenarios

HyunJun Jung^{*1}, Shun-Cheng Wu^{*1}, Patrick Ruhkamp^{*1}, Hannah Shieber², Pengyuan Wang¹, Giulia Rizzoli³, Hongcheng Zhao¹, Sven Damian Meier⁴, Daniel Roth², Nassir Navab¹, Benjamin Busam¹

¹ Technical University of Munich

² Friedrich-Alexander Universität (FAU) Erlangen-Nürnberg

³ University of Padova

⁴ Toyota Motor Europe

^{*} Equal Contribution

hyunjun.jung@tum.de

shuncheng.wu@tum.de

p.ruhkamp@tum.de

b.busam@tum.de



Figure 1. HouseCat6D is a multi-modal category level 6D object pose dataset with highly diverse household object categories with different photometric complexity and a high number of varying scenes covering large viewpoint distributions. An external tracking system enables for room-scale high quality camera tracking and object pose annotations without markers in the scene for realistic scenarios and trajectories. Our handheld multi-modal camera rig records synchronized RGB, depth from active stereo, and polarimetric RGB+P images of scenes comprising objects without texture, strong reflections, or translucency.

Abstract

Estimating the 6D pose of objects is one of the major fields in 3D computer vision. Since the promising outcomes from instance-level pose estimation, the research trends are heading towards category-level pose estimation for more practical application scenarios. However, unlike well-established instance-level pose datasets, available category-level datasets lack annotation quality and provided pose quantity. We propose the new category level 6D pose dataset **HouseCat6D** featuring 1) Multi-modality of Polarimetric RGB+P and Depth, 2) Highly diverse 194 objects of 10 household object categories including 2 photometrically challenging categories, 3) High-quality pose annotation with an error range of only 1.35 mm to 1.74 mm, 4) 41 large scale scenes with extensive viewpoint coverage, 5) Checkerboard-free environment throughout the en-

tire scene. We also provide benchmark results of state-of-the-art category-level pose estimation networks.

1. Introduction

6D pose estimation is one of the cornerstones in many computer vision tasks, especially for interactions like robotic grasping [51, 54] or augmented reality [14]. Many methods have been proposed to solve this task from various perspectives and achieve outstanding results on public benchmarks [4, 20, 28, 52]. Most of the methods focus on instance-level where each network is trained and tested on a single object instance [34, 48]. However, generalization and applicability are limited, as the object mesh is required, and an individual network needs to be trained for each instance. Recent methods focus on category-level

Dataset	RGB	Depth	Polarisation	Real	Multi-View	mm-accurate GT	Occlusion	Symmetry	Transparent	Reflective	Pose Density	Pose Variation	Workspace	Categories	Objects	Scenes	License
FAT [45]	✓	✓			✓	✓	✓	✓						–	21	> 1k	CC BY-NC-SA 4.0
BlenderProc [9]	✓	✓			✓	✓	✓	✓						–	–	> 1k	GNU GPL 3.0
LabelFusion [38]	✓	✓		✓			✓							–	12	138	BSD 3-Clause
Toyota Light [22]	✓	✓		✓				✓						–	21	21	MIT
YCB [4, 52]	✓	✓		✓			✓	✓						–	21	92	MIT
Linemod [2, 20]	✓	✓		✓			✓	✓						–	15	15	CC BY 4.0
GraspNet-1Billion [15]	✓	✓		✓			✓	✓						–	88	190	CC BY-NC-SA 4.0
T-LESS [21]	✓	✓		✓			✓	✓						–	30	20	CC BY 4.0
HomebrewedDB [28]	✓	✓		✓			✓	✓						–	33	13	CC0 1.0 Universal
ITODD [12]		✓			✓	✓	✓	✓		(✓)				–	28	800	CC BY-NC-SA 4.0
StereoOBJ-1M [32]	✓			✓	✓	✓	✓	✓	✓		++++	++++	+++	–	18	183	MIT
kPAM [37]	✓	✓		✓			✓	✓						2	91	362	MIT
CAMERA25 [49]	✓	✓		(✓)			✓							6	42	30	MIT
REAL275 [49]	✓	✓		✓			✓	✓						6	42	13	MIT
TOD [33]	✓	✓		✓	✓	✓		✓	✓					3	20	10	CC BY 4.0
Wild6D [16]	✓	✓		✓	✓			✓	(✓)		++	++	++++	–	162	N/A	Not specified
NOCS [49]	✓	✓		✓	✓						+	+	++	6	42	18	Non-Commercial
PhoCal [50]	✓	✓	✓	✓	✓	✓	✓	✓	✓	✓	+++	+++	+	8	60	24	CC BY 4.0
HouseCat6D (Ours)	✓	✓	✓	✓	✓	✓	✓	✓	✓	✓	+++++	+++++	+++++	10	194	41	CC BY 4.0

Table 1. **Dataset Overview.** HouseCat6D represents a large-scale and highly accurate category-level 6D pose dataset that combines the advantages of various established datasets (e.g. extensive pose coverage with highly accurate annotations).

pose estimation [7, 31, 35, 36, 49] by training on multiple objects within one category. They can later generalize to unseen objects from the same category. However, a significant limitation blocking further progress is the lack of datasets for training and evaluation that fulfills all criteria like: large-scale, accurate and realistic. Existing category-level datasets only comply partly, e.g. high quantity and low quality [49], or high quality but insufficient quantity [50].

To this end, we propose a new category-level dataset HouseCat6D. It consists of high-quality ground-truth annotations on greatly diverse objects acquired by multiple sensor modalities with extensive viewpoint coverage. Our dataset includes 194 objects from 10 different categories, including photometrically challenging classes such as glass and cutlery (Fig. 1), and 3 sensor modalities, *i.e.* RGB, depth, and polarimetric images, with a total of 23.5k frames and approx. 160k annotated object poses. Our dataset recording relies on an accurate external infrared tracking system and additional subsequent post-processing through sparse bundle adjustment to avoid errors induced by timestamp offsets and motion blur of the freely moving camera rig [41, 42]. Specifically, we conduct three calibrations, *i.e.* pivot calibration, timestamp calibration, and hand-eye-calibration. For the timestamp calibration, we adopt existing methods [13, 24] adjusted to our setup with an ICP-based method. For the hand-eye-calibration, we improve the calibration from recent work [50], by aggregating multiple measurements of a ChArUcO [1] calibration board (cf. Sec. 3.4). Compared to the recent PhoCal dataset [50]

that relies on a robotic end-effector to estimate poses and thus has limited viewpoint coverage and backgrounds, our method provides accurate object pose annotation and wide viewpoint coverage while providing pose annotations with similar quality. We use active stereo as depth maps which is more reliable on different surface materials [26, 50]. In addition to the typical RGB and depth, we provide polarimetric images with four different filter angles. Recent investigations have shown that this modality is especially suitable for tasks such as depth and surface normal estimation [27, 29, 47], and 6D pose estimation [17], especially for photometrically challenging objects or surfaces.

In summary, our main contributions are: (1) We propose HouseCat6D a large scale category-level object pose dataset comprising, which is *multi-modal* (RGBD + RGBP), comprising 194 high-quality 3D models of household objects including transparent and reflective objects in 41 sequences with broad viewpoint coverage and realistic scenarios without markers in the scene. (2) We develop a novel pipeline for annotation, recording, and accuracy-dependent post-processing to achieve comparable accuracy to a robotic GT [50], but with a handheld multi-camera rig to enable realistic camera trajectories. (3) We detail the pose annotation pipeline with a commonly used external IR tracking system together with calibration details and its evaluation, which makes the high-quality 6D pose dataset annotation accessible to the community. (4) We provide and discuss the benchmark evaluation results on HouseCat6D for the SOTA category-level baselines NOCS [49], FS-Net [8], and

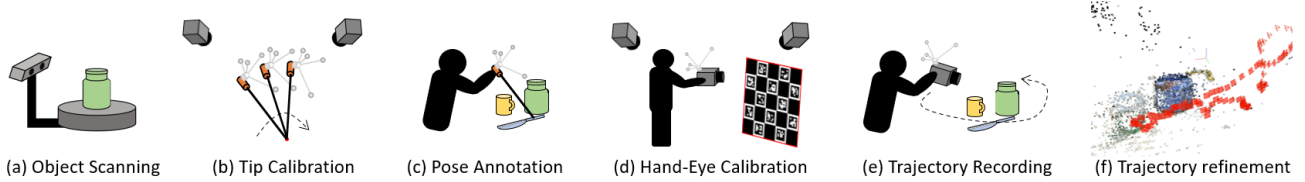


Figure 2. **Dataset Acquisition Pipeline.** (a): Pre-scanning 3D models. (b): Pivot calibration to calibrate measurement tip from the tracking body. (c): Pose annotation of objects using measurement tip. (d): Hand-Eye-Calibration to calibrate camera center of tracking body. (e): Camera trajectory recording (f): Post-processing step to reduce synchronization-induced trajectory error.

GPV-Pose [10] for scientifically meaningful insights and to foster novel research in the field.

2. Related Work

The field of 6D pose estimation can be broadly divided into two sub-fields: Instance-level 6D pose estimation and category-level 6D pose estimation. The former focuses on estimating the pose of a single object, and the latter focuses on estimating the pose of object within the same class. The recent state-of-the-art methods are mostly data-driven approaches. A common need for these methods are datasets for both training and evaluation. In this section, we give an overview of previous datasets.

2.1. Instance-level 6D Object Pose Dataset

Early 6D pose datasets started from a single image (*i.e.* images are not in sequence). LineMOD [20] and LM-Occlusion [2] are amongst the most popular and commonly used datasets, for instance, level pose estimation. An RGBD camera is used to annotate the pose of the objects, and checkerboards are used to track the camera pose. Although these two datasets served an essential role in the early time, they have limitations in terms of their annotation quality [3] and the quality of the provided object meshes. Later, HomebrewedDB [28] is released with 33 high-quality 3D objects scanned by a commercial hand-held scanner to resolve the issues of object meshes. Although HomebrewedDB [28] features better quality for object mesh and pose annotation, it lacks scene variety. Only 13 scenes are provided, and checkerboards are included in the scenes. A variety of pose datasets share similar principal [11, 43]. RGBD-based annotation is typically used with checkerboard-based camera localization, sometimes with different objects of interest [21]. Other works use human-powered annotation [40] or a rotating table [12] instead of checkerboards.

Lately, more datasets have provided image sequences with camera and object pose annotations. With video sequences, the pose estimation problem can be simplified to pose tracking [3, 18, 30]. One of the most widely used 6D pose datasets with video sequences is YCB [52]. The authors annotate the pose by leveraging an RGBD cam-

era and structure from motion (Label Fusion [38]). While this makes large-scale annotation possible, the dataset suffers from depth-induced error [3, 50], making the annotation quality bound to the commercial depth camera used. In comparison, the Laval 6DOF dataset [18] uses a different approach, which attaches small markers on the objects for tracking purposes while the camera is fixed. This results in high-quality annotations without checkerboards. However, marker-induced depth artifacts need a depth map post-correction. On the other hand, StereoOBJ-1M [32] uses structure from motion in a more precise way together with the use of checkerboards to ensure quality and quantity. This allows the dataset to be the largest available pose dataset in scale with high-quality annotation (cf. Tab. 2).

2.2. Category-level Object Poses and Dataset

Category-level pose estimation has been proposed to address generalizability in 6D pose estimation over multiple objects of the same category. The task is to generalize pose estimation per class and not for individual instances, which is challenging due to high intra-class variance.

Wang *et al.* [49] present NOCS, an approach, and dataset for category-level 6D pose and size estimation. It contains six categories and two datasets: a mixed reality dataset (CAMERA25) and a real RGB-D dataset (REAL275). In REAL275, the poses are aligned using checkerboards. For CAMERA25, ShapeNetCore [5] objects are placed in tabletop scenarios. To estimate the pose on NOCS, they adapt Mask R-CNN [19] to predict the normalized object coordinate space (NOCS) maps and instance mask. This prediction is combined with the depth image to lift the prediction to 3D. Several approaches have been proposed on NOCS data to tackle the challenge of 6D pose estimation (*i.e.* [6, 8, 10, 25, 31, 35, 36, 44]). FS-Net [8] utilizes graph convolutions to encode the object shapes, and predicts the pose using a decoupled rotation mechanism. GPV-Pose [10] further improves FS-Net [8] by adding geometry awareness through a geometric consistency loss which optimizes between 3D bounding boxes, reconstruction, and poses. While they rely on bounding box predictions or semantic segmentation masks, Centersnap [25] is free of bounding boxes or segmentation masks and predicts in a single-stage

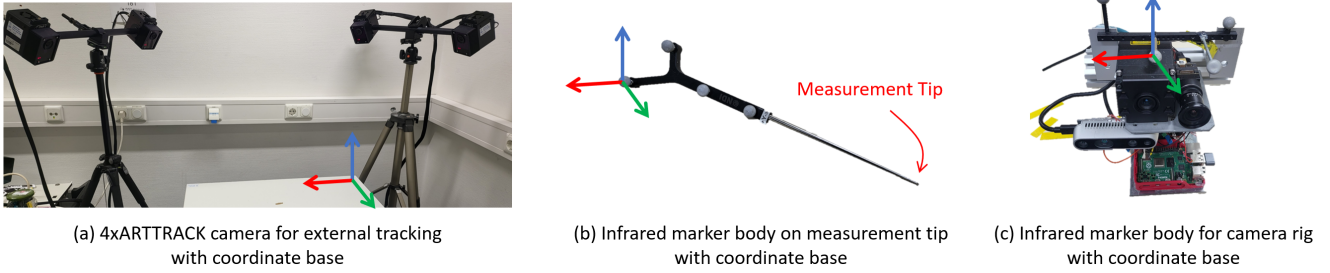


Figure 3. **Tracking System.** ARTTRACK2 tracking system and sets of infrared marker bodies we used for our setup. Once at least four infrared spheres are detected from at least two cameras, the tracking system provides the pose of the marker body as transformation from tracker system base to marker body base.

the 3D shape, 6D pose, and size of the objects in one network.

A dataset focusing more on the robotic field is kPam which uses keypoints. Manuelli *et al.* [37] capture kPam using a similar approach as [38]. They perform 3D reconstruction before manually labeling the keypoints on the 3D reconstruction. The dataset results in 117 training sequences and 245 testing sequences.

While NOCS and kPAM contain solid objects, TOD [33] and PhoCal [50] specifically focus on either translucent or transparent and reflective objects. TOD [33] is captured with a robotic arm and annotated keypoints and focuses on stereo images. Wang *et al.* [50] introduce a category-level dataset including polarimetric images besides RGBD only. For annotation, a robotic arm is used to tip individual objects with a calibrated pointer. Annotations are refined via ICP.

Instead of using a robotic arm, Wild6D [16] is annotated via tracking. Every 50th keyframes is annotated and then registered via TEASER++ [53] and colored ICP [39]. The training dataset is label-free, and only the test dataset contains annotations. For recording, multiple iPhones are used to capture RGB images, depth, and point cloud. As a baseline, Fu *et al.* [16] introduce RePoNet, which estimates pose, NOCS map, and shape via pose and shape networks connected with a differentiable rendering module. We summarize the mentioned datasets in Tab. 1.

3. Dataset

Our dataset aims at large scale with large view coverage and high quality pose annotation without the use of a checkerboard. It is composed of 34 training scene (20k frames), five test scenes (3k frames) and two validation scenes (1.4k frames). The scenes comprise objects from 10 household categories including photometrically challenging objects, such as glass and cutlery. With a total of 194 objects, each category contains 19 objects in average. Our dataset also features multiple modalities, namely RGB images, polarimetric images and depth maps. This section de-

tails our dataset. The acquisition setup is described briefly in Fig. 2.

3.1. Objects Mesh Acquisition

For our dataset, we choose 10 household categories to represent typical household scenarios. These are: bottle, box, can, cup, cutlery, glass, remote, shoe, teapot, tube. Similar to [50], all objects are scanned with high quality EinScan-SP 3D Scanner (SHINING 3D Tech. Co., Ltd., Hangzhou, China), which has a structured light stereo system with a single shot accuracy of ≤ 0.05 mm in a scanning volume of $1200 \times 1200 \times 1200$ mm³. For the photometrically challenging categories, we use self-vanishing 3D scanning spray (AESUB Blue, Aesub, Recklinghausen, Germany) to enable scanning. We provide meshes of all objects as obj-file.

3.2. Hardware

External Tracking System. To ensure broad viewpoint coverage with high-quality annotation without using a checkerboard, we utilize an external tracker system composed of four ARTTRACK2 cameras (Advanced Realtime Tracking GmbH & Co, Germany) with built-in infrared flash (NIR, 880 nm) and maximum tracking distance of 4.5 m for both object pose and camera pose annotation. Fig. 3 shows our camera setup and used tracking bodies for the annotation pipeline. We evaluate the accuracy of the tracking setup as translation and rotational error [18] using a robotic setup (details in supplementary material). This results in an average 0.67 mm / 0.12° error in the static case and 0.92 mm / 0.16° error in the dynamic tracking scenario.

Cameras. Our multi-modal dataset comprises two main modalities: Polarimetric RGB image and active stereo depth. A Phoenix 5.0 MP Polarization camera with Sony IMX264MYR CMOS Polarsens (PHX050S1-QC, LUCID Vision Labs, Inc., Canada) sensor is used to produce the RGB+P images, and Intel RealSense D435 (RealSense

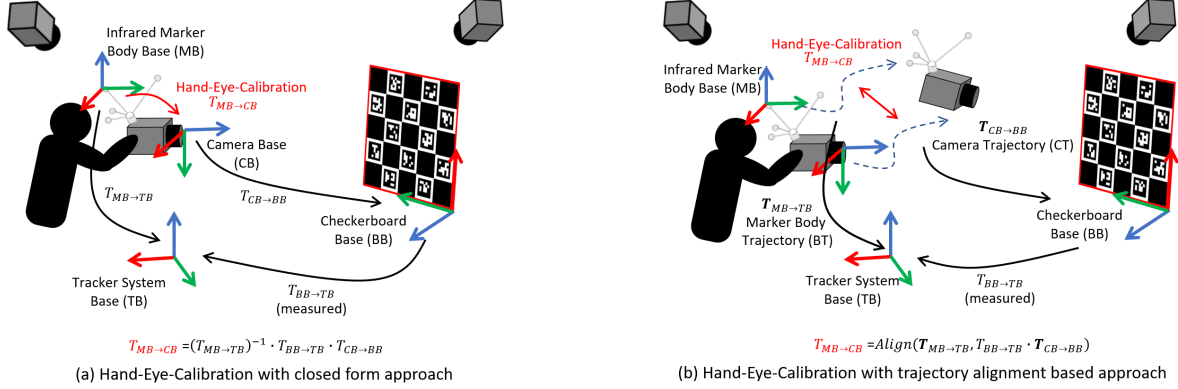


Figure 4. **Hand-Eye-Calibration.** Overview of two hand-eye-calibration methods which leverage the measured pose of the checkerboard. Although close form approach (a) produces good quality calibration, the quality of the calibration highly depends on the quality of the checkerboard detection and camera trajectory quality deviates when the camera pose deviates from the pose used for the calibration. Our newly proposed approach (b) takes more image captures into account. This makes it more robust against checkerboard detection error in a wider range of camera poses.

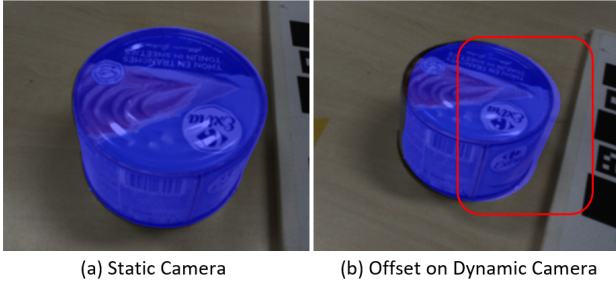


Figure 5. **Camera Synchronisation Effect.** Compared to a static scene (a), camera synchronization effects produce an offset in a dynamic scene (b). If we retrieve the camera pose from an unsynchronized timestamp severe errors on the camera pose are visible.

D435i, Intel, USA) acquires the depth maps. We specifically choose D435 as the depth sensor over Time-of-Flight sensors as active stereo depth provides, in general, more robust depth on photometrically challenging material [26]. To ensure the best synchronization between the two cameras, we use an external tracking signal provided by a Raspberry Pi (Raspberry Pi Foundation, United Kingdom) with GPIO output and later use the trigger signal as the timestamp of images for post-ex synchronization correction with the tracking system.

3.3. Object Pose Annotation

Annotating the 6D pose of the object is, without a doubt, the most crucial part of a 6D pose dataset. In our dataset, we adopt the highly accurate object pose annotation pipeline from [50] by replacing the robotic end-effector pose with an IR tracking body. This ensures reliable tracking quality while covering a more extensive working volume. The annotation step follows tool tip calibration, 3D points mea-

surement of the objects, and point correspondence with ICP-based refinement. In this subsection, we describe the details of each step.

Tip Calibration. The poses of the object meshes are annotated by measuring the 3D point using the tool tip. Thus, calibrating the location of the tip from the tracking body is essential to ensure the accuracy of the annotation. We use an NDI Active 4-Marker Planar Rigid Body (Northern Digital, Ontario Canada) as the measurement tip (Fig. 3 (b)). The tip is calibrated by fixing the tip while pivoting the tracking body and finding the optimal location of the point to minimize the variance of the fixed point (pivot calibration). The most common way to evaluate the quality of the pivot calibration is by measuring the variance of the fixed pivot point. We carefully calibrated with 18 points, with the final variance of the tip location of $\varepsilon = 0.040$ mm.

Pose Annotation. After the tip is calibrated from the tracking body, it can measure accurate 3D points in the space in the world coordinates of the tracker system. We measure points for the initial point correspondence and ICP refinement as in [50] while covering around three times more points measurements with various surfaces of the object, thanks to the enlarged working space without the constraint given by using a robot arm [50]. We evaluate the quality of the pose annotation step by simulating the pose annotation pipeline on randomly selected three objects with the addition of pivot calibration error (Sec. 3.3) and static tracking error (Sec. 3.2), which gives an average RMSE of 0.32 mm in translation and 0.43° in rotation.

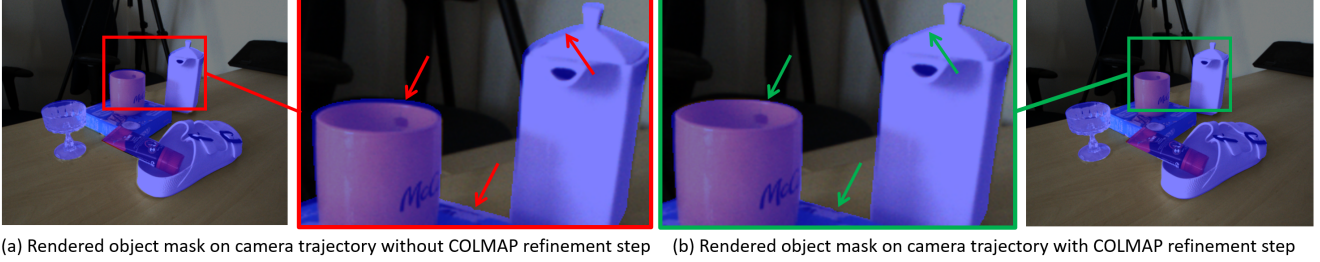


Figure 6. **Post-Processing via Bundle Adjustment.** Example of COLMAP [41, 42] refinement on selected frame with large camera displacement. Even though out timestamp synchronization step reduces the effect of motion induced pose offset, subtle errors still remain ((a), marked red). In comparison, the post processing step significantly reduces the given offset error ((b), marked green).

3.4. Camera Trajectory Annotation

Another critical aspect of 6D pose dataset annotation are accurate camera trajectories. The object poses are annotated from the center of the tracker system, not from the center of the individual camera. Thus, the camera pose from the tracker system base has to be applied to obtain the 6D pose of the object from the camera center. In this section, we describe the detailed steps of camera trajectory annotation in a precise way.

Hand-Eye-Calibration In our scenario, Hand-Eye-Calibration obtains the transformation between the tracker marker body and the center of the camera image sensor. The most common way to perform Hand-Eye-Calibration is by detecting the checkerboard via camera while tracking the body of the camera from an external source. In [46], they detect the checkerboard many times and optimize both the checkerboard base from the tracker system base $T_{BB \rightarrow TB}$ and camera base from the marker body base $T_{MB \rightarrow CB}$ (hand-eye-calibration). The recent work [50] proposes a way to leverage the measurement tip to measure $T_{BB \rightarrow TB}$ to make the optimization process simpler (Fig. 4 (a)). However, we found that the accuracy of the closed-form solution is often unreliable. To solve this issue, we propose a new hand-eye-calibration, which takes into account multiple images captures (Fig. 4 (b)). Unlike [50], we capture multiple static images from different locations to form two trajectories - one from the camera and one from the tracking body. The fixed transformation between these two trajectories is the hand-eye-calibration matrix, which we extract by applying Horn’s alignment method [23]. Once the calibration $T_{MB \rightarrow CB}$ is obtained, we align the two trajectories and compare the errors as the calibration accuracy. The RMSE for this calibration is measured as 0.27 mm for the translation and 0.42° for the rotation.

Camera to Tracker Time Synchronization Another important aspect of using the external IR tracking system is the timestamp calibration between the tracking system and

the camera image acquisition time. It can cause severe offset on poses depending on the movement of the camera, as illustrated in Fig. 5. A common practice to synchronize the timestamp difference is to measure the trajectory of the camera from two modalities, via image and tracking system, along with their timestamp, and maximize the similarity between the trajectories. This brings the best timestamp offset [13, 24]. In our case, we use ICP-based trajectory alignment to find the best timestamp offset instead of using a similarity measure. We empirically find it is more robust to noise and able to synchronize two trajectories with arbitrary frequency without any interpolation to match the frequency. For the camera timestamp, we use the hardware trigger timestamp from the raspberry pi instead of the image callback timestamp. This is because the image callback can vary with the cable, connection, and PC workload. We evaluate the synchronization by simulating two unsynchronized signals. One signal with the tracking system error (Sec. 3.2) to replicate the camera trajectory via the tracking system signal and the other with the detection based error (Sec. 3.4) to replicate the camera trajectory via the camera detection. The simulated error is measured as 0.03 sec.

Pose Refinement Although the time synchronization improves the quality of the camera pose, the motion-induced pose error cannot be obliterated as the time synchronization is imperfect due to the noise in the checkerboard detection during the calibration [24] as well as the difference in of individual camera image acquisition time due to its hardware condition. This effect can be observed when the camera motion involves large displacement between consecutive frames (Fig. 6,(a)). To tackle this issue, we use the RGB input to minimize the reprojection error with multi-view images. We use structure from motion [41, 42] with given initial poses and carefully selected fixed frames. The initial poses are used for initial feature matching and structure reconstruction. The fixed frames are excluded in the later bundle adjustment stage. These frames are manually picked upon careful inspection on the frame with the largest

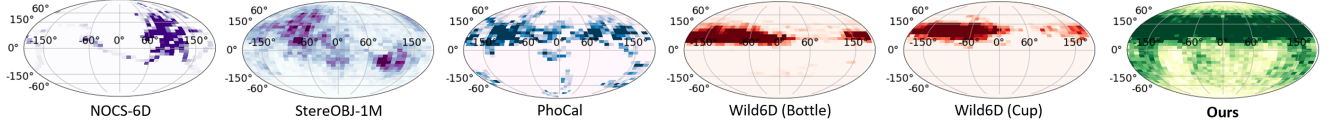


Figure 7. **Pose Distribution.** The pose distribution for category-level datasets NOCS [49] (Test), StereOBJ-1M [32] (Val), PhoCal [50] (Train), two categories of Wild6D [16] and Ours is plotted as the Mollweide projection of the spherical histogram, to exemplify the density and pose variation. Ours shows larger diversity of poses around objects, also for the lower hemisphere, and denser overall distribution.

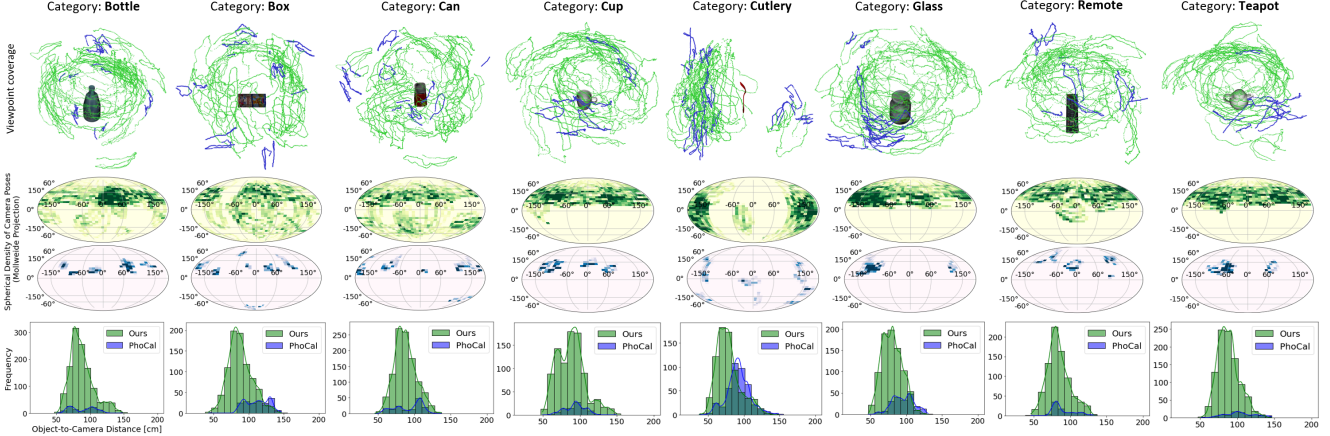


Figure 8. **Pose Distribution per Category.** We compare the pose distribution of HouseCat6D (green) against the very recent PhoCal [50] dataset (blue), for the categories included in both of them. The trajectory visualisation (top) verifies the much larger and better distributed pose coverage of our HouseCat6D dataset. Compared is further the rotational pose coverage as spherical histogram plotted as Mollweide projection (centre) and the object-to-camera distance as a histogram with relative frequency against the distance in cm (bottom).

Dataset	RGBD based	TOD [33]	StereOBJ [32]	PhoCal [50]	Ours
3D Labeling	Depth Map	Multi-View	Multi-View	Robot	IR tracker
Point RMSE	≥ 17 mm	3.4 mm	2.3 mm	0.80 mm	$1.35 \text{ mm} \leq \epsilon \leq 1.73 \text{ mm}$

Table 2. **Accuracy Comparison against existing Datasets.** RGBD-based datasets suffer from the standard deviation of the sensor [32]. Multi-view setups [32, 33] improve this. our annotation quality is lower than robotic acquisition [50], however, we cover significantly more viewpoints and provide more accurate annotations than checkerboard-based datasets [32].

IoU between rendered object mask on the RGB image given the pose annotation. Unlike other pipelines, this additional refinement step cannot be additionally evaluated, as knowing the improvement would require access to the absolute ground truth of the object pose. This can only be obtained in a fully synthetic rendering case, which suffers from a domain gap between synthetic and real-world images.

3.5. Annotation Quality Evaluation

For the evaluation of the annotation quality, we report the point-wise RMSE between objects and the camera center with and without the consideration of three systematic errors: tracking system error (Sec. 3.2), pose annotation error (Sec. 3.3) and hand-eye-calibration error (Sec. 3.4). As the accuracy gain from the structure-from-motion cannot be

directly quantified, we report the RMSE with upper- and lower bounds. In the upper bound, we report the number with the object annotation error and the static tracking error, assuming no synchronization error. In the lower bound, we include all tree mentioned systematic errors with dynamic tracking error as the tracking system error. We report our annotation quality compared to recent datasets in Tab. 2. Our method achieves low RMSE from 1.35 mm to 1.73 mm.

3.6. Scene Statistics

HouseCat6D features 41 large-scale scenes with 194 objects in 10 categories. It is composed of 34 training scenes with 124 objects, 5 test scenes with 50 objects and 2 validation scenes with 20 objects. For the 34 training scenes, a total of 20k frames are recorded. Each training scene contains on average 6 objects of different categories. On the other hand, 5 test scenes and 2 validation scenes consist of 3k and 1.4k frames. They are composed of 10 unseen objects per scene with different categories. Compared to other category-level datasets, our dataset covers the most diverse number of instances and categories.

3.7. Pose Coverage

Established datasets in 6D pose estimation are missing well-distributed and dense camera pose coverage around

Approach	3D ₂₅ / 3D ₅₀	Bottle	Box	Can	Cup	Remote	Teapot	Cutlery	Glass	Tube	Shoe
NOCS [49]	37.8 / 2.1	23.0 / 0.00	31.0 / 0.2	88.0 / 15.6	54.2 / 0.00	72.7 / 1.7	3.0 / 0.00	7.3 / 0.1	85.8 / 2.0	10.8 / 0.9	2.0 / 0.00
GPV-Pose [10]	68.3 / 36.2	65.0 / 43.2	31.9 / 15.9	99.3 / 78.5	90.8 / 49.1	62.8 / 46.6	66.3 / 53.0	41.3 / 11.5	96.7 / 21.2	73.0 / 15.7	52.3 / 34.0
FS-Net [8]	69.4 / 37.0	64.0 / 42.7	29.4 / 12.7	99.6 / 75.1	92.3 / 54.1	62.6 / 45.3	69.1 / 54.2	43.5 / 10.6	97.2 / 28.2	72.2 / 14.9	58.2 / 38.2

Table 3. **Quantitative Baseline Comparisons.** Class-wise evaluation of 3D IoU (at 25%/ at 50%) for NOCS [49], FS-Net [8], and GPV-Pose [10] on the test split of HouseCat6D.

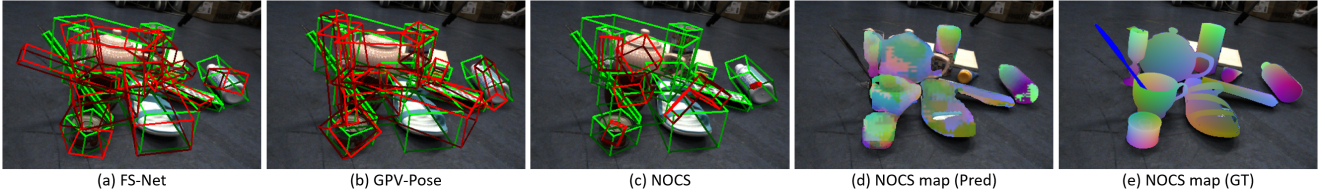


Figure 9. **Qualitative Baseline Comparisons and NOCS map.** Visualization of the baseline predictions on the test set of HouseCat6D for FS-Net [8], GPV-Pose [10] and NOCS [49] together with predicted NOCS map with GT NOCS map

the object. They usually focus on the upper hemisphere, even for large-scale dataset variants like SterOBJ-1M [32]. In contrast, HouseCat6D provides very dense and well-distributed poses (cf. Fig. 7). In terms of category level, we compare our trajectories for mutual classes against the recent PhoCal [50] dataset, which provides very accurate annotations, but is limited in the range of motion by the robotic arm used for acquisition (cf. Fig. 8).

4. Benchmark and Experiments

Commonly used in 6D pose estimation are RGB-D approaches like NOCS [49]. RGB provides information about the object itself (the class). However, categories can show a high intra-class variance. Thus, the RGB image is first used to identify the object and depth is leveraged consecutively to learn more about the shape and object boundaries. NOCS [49] predicts NOCS maps in 2D image space and utilizes depth information and ICP for 3D prediction. Similarly, GPV-Pose first segments the object in the RGB image and then applies back-projection of the segmented depth map to the 3D space where it predicts the pose using geometry-guided point-wise voting. FS-Net [8] extracts the 3D point cloud from the depth image based on 2D RGB object detection. From this, latent features are extracted using a residual network, and object size and translation are estimated. For our experiment using FS-Net [8], we follow the implementation of Di *et al.* [10].

4.1. Evaluation Pipeline & Results

Our dataset consists of 34 training sequences, 2 validation sequences, and 5 test sequences. For the baseline results, we report the results on the test split. We report the intersection over union (IoU) result with a threshold of 25% and 50%. NOCS [49] results in a mean average precision (mAP) of 37.8 for 3D IoU at 25%. The geometry-guided

approach GPV-Pose [10] gives 68.3% mAP for 3D IoU at 25%. FS-Net [8] achieves the best average results with an mAP of 69.4% for 3D IoU at 25%. Class-wise comparisons are listed in Tab. 3.

Compared to the widely used NOCS [49] dataset, our data contains cluttered scenes which lead to occluded object parts and objects in close proximity to each other as illustrated in Fig. 9. Current category-level 6D pose estimation pipelines mostly consider cases without occlusion. This leaves room for improvement as can be seen by this first evaluation. Fig. 9 (d), (e) furthermore indicate that NOCS is challenged by the glass. Also, the object behind the teapot handle cannot be fully recovered.

5. Discussion and Conclusion

We have introduced HouseCat6D, a large-scale 6D pose dataset acquired with a custom multi-modal camera rig with an external tracking system, which provides highly accurate pose annotations. With this setup, we solve issues of established datasets by providing realistic scenes without markers for which object poses are well distributed in realistic scenarios. Additionally, our annotation approach allows us to include photometrically challenging objects without texture and with translucent material. On the other hand, our dataset has a few drawbacks from the limitation of the tracking system. First, it requires a manual annotation that is labor-intensive and time-consuming. This makes scaling the magnitude of the dataset difficult. Second, our tracking system limits the scene recording to indoor scenes as the system does work under strong sunlight. However, with the given quality and quantity of the dataset, HouseCat6D overcomes the aforementioned shortcomings and fosters novel research and development in the field of categorical pose estimation. HouseCat6D, therefore, paves the way for pose applications in everyday household situations.

References

- [1] Gwon Hwan An, Siyeon Lee, Min-Woo Seo, Kugjin Yun, Won-Sik Cheong, and Suk-Ju Kang. Charuco board-based omnidirectional camera calibration method. *Electronics*, 7(12):421, 2018.
- [2] Eric Brachmann, Alexander Krull, Frank Michel, Stefan Gumhold, Jamie Shotton, and Carsten Rother. Learning 6d object pose estimation using 3d object coordinates. In *Proceedings of the European Conference on Computer Vision*, pages 536–551. Springer, 2014.
- [3] Benjamin Busam, Hyun Jun Jung, and Nassir Navab. I like to move it: 6d pose estimation as an action decision process. *arXiv preprint arXiv:2009.12678*, 2020.
- [4] Berk Calli, Aaron Walsman, Arjun Singh, Siddhartha Srinivasa, Pieter Abbeel, and Aaron M Dollar. Benchmarking in manipulation research: The ycb object and model set and benchmarking protocols. *arXiv preprint arXiv:1502.03143*, 2015.
- [5] Angel X Chang, Thomas Funkhouser, Leonidas Guibas, Pat Hanrahan, Qixing Huang, Zimo Li, Silvio Savarese, Manolis Savva, Shuran Song, Hao Su, et al. Shapenet: An information-rich 3d model repository. *arXiv preprint arXiv:1512.03012*, 2015.
- [6] Dengsheng Chen, Jun Li, Zheng Wang, and Kai Xu. Learning canonical shape space for category-level 6d object pose and size estimation. In *Proceedings of the IEEE/CVF conference on computer vision and pattern recognition*, pages 11973–11982, 2020.
- [7] Wei Chen, Xi Jia, Hyung Jin Chang, Jinming Duan, Linlin Shen, and Ales Leonardis. Fs-net: Fast shape-based network for category-level 6d object pose estimation with decoupled rotation mechanism. In *Proceedings of the IEEE/CVF Conference on Computer Vision and Pattern Recognition*, pages 1581–1590, 2021.
- [8] Wei Chen, Xi Jia, Hyung Jin Chang, Jinming Duan, Linlin Shen, and Ales Leonardis. Fs-net: Fast shape-based network for category-level 6d object pose estimation with decoupled rotation mechanism. In *Proceedings of the IEEE/CVF Conference on Computer Vision and Pattern Recognition (CVPR)*, pages 1581–1590, June 2021.
- [9] Maximilian Denninger, Martin Sundermeyer, Dominik Winkelbauer, Dmitry Olefir, Tomas Hodan, Youssef Zidan, Mohamad Elbadrawy, Markus Knauer, Harinandan Katam, and Ahsan Lodhi. Blenderproc: Reducing the reality gap with photorealistic rendering. In *International Conference on Robotics: Science and Systems, RSS 2020*, 2020.
- [10] Yan Di, Ruida Zhang, Zhiqiang Lou, Fabian Manhardt, Xi-angyang Ji, Nassir Navab, and Federico Tombari. Gpv-pose: Category-level object pose estimation via geometry-guided point-wise voting. In *Proceedings of the IEEE/CVF Conference on Computer Vision and Pattern Recognition*, pages 6781–6791, 2022.
- [11] Andreas Doumanoglou, Rigas Kouskouridas, Sotiris Malasiotis, and Tae-Kyun Kim. Recovering 6d object pose and predicting next-best-view in the crowd. In *Proceedings of the IEEE Conference on Computer Vision and Pattern Recognition*, pages 3583–3592, 2016.
- [12] Bertram Drost, Markus Ulrich, Paul Bergmann, Philipp Hartinger, and Carsten Steger. Introducing mvtec itodd - a dataset for 3d object recognition in industry. In *Proceedings of the IEEE International Conference on Computer Vision Workshops*, Oct 2017.
- [13] Ulrich Eck, Frieder Pankratz, Christian Sandor, Gudrun Klinker, and Hamid Laga. Precise haptic device co-location for visuo-haptic augmented reality. *IEEE Transactions on Visualization and Computer Graphics*, 0:15, 09 2015.
- [14] Marco Esposito, Benjamin Busam, Christoph Hennesperger, Julia Rackerseder, Nassir Navab, and Benjamin Frisch. Multimodal us-gamma imaging using collaborative robotics for cancer staging biopsies. *International journal of computer assisted radiology and surgery*, 11(9):1561–1571, 2016.
- [15] Hao-Shu Fang, Chenxi Wang, Minghao Gou, and Cewu Lu. Graspnet-1billion: A large-scale benchmark for general object grasping. In *Proceedings of the IEEE/CVF conference on computer vision and pattern recognition*, pages 11444–11453, 2020.
- [16] Yang Fu and Xiaolong Wang. Category-level 6d object pose estimation in the wild: A semi-supervised learning approach and a new dataset. *arXiv:2206.15436*, 2022.
- [17] Daoyi Gao, Yitong Li, Patrick Ruhkamp, Iuliia Skobleva, Magdalena Wysock, HyunJun Jung, Pengyuan Wang, Arturo Guridi, and Benjamin Busam. Polarimetric pose prediction, 2021.
- [18] Mathieu Garon, Denis Laurendeau, and Jean-François Lalonde. A framework for evaluating 6-DOF object trackers. In *Proceedings of the European Conference on Computer Vision*, 2018.
- [19] Kaiming He, Georgia Gkioxari, Piotr Dollar, and Ross Girshick. Mask r-cnn. In *Proceedings of the IEEE International Conference on Computer Vision (ICCV)*, Oct 2017.
- [20] Stefan Hinterstoisser, Stefan Holzer, Cedric Cagniart, Slobodan Ilic, Kurt Konolige, Nassir Navab, and Vincent Lepetit. Multimodal templates for real-time detection of texture-less objects in heavily cluttered scenes. In *Proceedings of the IEEE International Conference on Computer Vision*, pages 858–865. IEEE, 2011.
- [21] Tomáš Hodan, Pavel Haluza, Štěpán Obdržálek, Jiri Matas, Manolis Lourakis, and Xenophon Zabulis. T-less: An rgb-d dataset for 6d pose estimation of texture-less objects. In *2017 IEEE Winter Conference on Applications of Computer Vision (WACV)*, pages 880–888. IEEE, 2017.
- [22] Tomas Hodan, Frank Michel, Eric Brachmann, Wadim Kehl, Anders GlentBuch, Dirk Kraft, Bertram Drost, Joel Vidal, Stephan Ihrke, Xenophon Zabulis, et al. Bop: Benchmark for 6d object pose estimation. In *Proceedings of the European conference on computer vision (ECCV)*, pages 19–34, 2018.
- [23] Berthold Horn, Hugh Hilden, and Shahriar Negahdaripour. Closed-form solution of absolute orientation using orthonormal matrices. *Journal of the Optical Society of America A*, 5:1127–1135, 07 1988.
- [24] Manuel Huber, Michael Schlegel, and Gudrun Klinker. Temporal calibration in multisensor tracking setups. In *2009 8th IEEE International Symposium on Mixed and Augmented Reality*, pages 195–196. IEEE, 2009.

- [25] Muhammad Zubair Irshad, Thomas Kollar, Michael Laskey, Kevin Stone, and Zsolt Kira. Centersnap: Single-shot multi-object 3d shape reconstruction and categorical 6d pose and size estimation. In *2022 International Conference on Robotics and Automation (ICRA)*, pages 10632–10640, 2022.
- [26] HyunJun Jung, Patrick Ruhkamp, Guangyao Zhai, Nikolas Brasch, Yitong Li, Yannick Verdie, Jifei Song, Yiren Zhou, Anil Armagan, Slobodan Ilic, Ales Leonardis, and Benjamin Busam. Is my depth ground-truth good enough? hammer – highly accurate multi-modal dataset for dense 3d scene regression, 2022.
- [27] Agastya Kalra, Vage Taamazyan, Supreeth Krishna Rao, Kartik Venkataraman, Ramesh Raskar, and Achuta Kadambi. Deep polarization cues for transparent object segmentation. In *Proceedings of the IEEE Conference on Computer Vision and Pattern Recognition*, pages 8602–8611, 2020.
- [28] Roman Kaskman, Sergey Zakharov, Ivan Shugurov, and Slobodan Ilic. Homebreweddb: Rgb-d dataset for 6d pose estimation of 3d objects. *Proceedings of the IEEE International Conference on Computer Vision Workshops*, 2019.
- [29] Chenyang Lei, Chenyang Qi, Jiaxin Xie, Na Fan, Vladlen Koltun, and Qifeng Chen. Shape from polarization for complex scenes in the wild, 2021.
- [30] Yi Li, Gu Wang, Xiangyang Ji, Yu Xiang, and Dieter Fox. DeepIM: Deep iterative matching for 6d pose estimation. *International Journal of Computer Vision*, 128(3):657–678, nov 2019.
- [31] Jiehong Lin, Zewei Wei, Zhihao Li, Songcen Xu, Kui Jia, and Yuanqing Li. Dualposenet: Category-level 6d object pose and size estimation using dual pose network with refined learning of pose consistency. In *Proceedings of the IEEE/CVF International Conference on Computer Vision*, pages 3560–3569, 2021.
- [32] Xingyu Liu, Shun Iwase, and Kris M Kitani. Stereobj-1m: Large-scale stereo image dataset for 6d object pose estimation. In *Proceedings of the IEEE International Conference on Computer Vision*, pages 10870–10879, 2021.
- [33] Xingyu Liu, Rico Jonschkowski, Anelia Angelova, and Kurt Konolige. Keypose: Multi-view 3d labeling and keypoint estimation for transparent objects. In *Proceedings of the IEEE Conference on Computer Vision and Pattern Recognition*, pages 11602–11610, 2020.
- [34] Fabian Manhardt, Diego Martin Arroyo, Christian Rupprecht, Benjamin Busam, Tolga Birdal, Nassir Navab, and Federico Tombari. Explaining the ambiguity of object detection and 6d pose from visual data. In *Proceedings of the IEEE/CVF International Conference on Computer Vision*, pages 6841–6850, 2019.
- [35] Fabian Manhardt, Manuel Nickel, Sven Meier, Luca Minciullo, and Nassir Navab. Cps: Class-level 6d pose and shape estimation from monocular images. *arXiv preprint arXiv:2003.05848*, 2020.
- [36] Fabian Manhardt, Gu Wang, Benjamin Busam, Manuel Nickel, Sven Meier, Luca Minciullo, Xiangyang Ji, and Nassir Navab. Cps++: Improving class-level 6d pose and shape estimation from monocular images with self-supervised learning. *arXiv preprint arXiv:2003.05848*, 2020.
- [37] Lucas Manuelli, Wei Gao, Peter Florence, and Russ Tedrake. kpam: Keypoint affordances for category-level robotic manipulation. In *The International Symposium of Robotics Research*, pages 132–157. Springer, 2019.
- [38] Pat Marion, Peter R Florence, Lucas Manuelli, and Russ Tedrake. Label fusion: A pipeline for generating ground truth labels for real rgbd data of cluttered scenes. In *IEEE International Conference on Robotics and Automation*, pages 3235–3242. IEEE, 2018.
- [39] Jaesik Park, Qian-Yi Zhou, and Vladlen Koltun. Colored point cloud registration revisited. In *Proceedings of the IEEE international conference on computer vision*, pages 143–152, 2017.
- [40] Colin Rennie, Rahul Shome, Kostas E Bekris, and Alberto F De Souza. A dataset for improved rgbd-based object detection and pose estimation for warehouse pick-and-place. *IEEE Robotics and Automation Letters*, 1(2):1179–1185, 2016.
- [41] Johannes Lutz Schönberger and Jan-Michael Frahm. Structure-from-motion revisited. In *Conference on Computer Vision and Pattern Recognition (CVPR)*, 2016.
- [42] Johannes Lutz Schönberger, Enliang Zheng, Marc Pollefeys, and Jan-Michael Frahm. Pixelwise view selection for unstructured multi-view stereo. In *European Conference on Computer Vision (ECCV)*, 2016.
- [43] Alykhan Tejani, Danhang Tang, Rigas Kouskouridas, and Tae-Kyun Kim. Latent-class hough forests for 3D object detection and pose estimation. In *Proceedings of the European Conference on Computer Vision*, pages 462–477. Springer, 2014.
- [44] Meng Tian, Marcelo H Ang, and Gim Hee Lee. Shape prior deformation for categorical 6d object pose and size estimation. In *European Conference on Computer Vision*, pages 530–546. Springer, 2020.
- [45] Jonathan Tremblay, Thang To, and Stan Birchfield. Falling things: A synthetic dataset for 3d object detection and pose estimation. In *Proceedings of the IEEE Conference on Computer Vision and Pattern Recognition Workshops*, pages 2038–2041, 2018.
- [46] Roger Y Tsai, Reimar K Lenz, et al. A new technique for fully autonomous and efficient 3 d robotics hand/eye calibration. *IEEE Transactions on robotics and automation*, 5(3):345–358, 1989.
- [47] Yannick Verdié, Jifei Song, Barnabé Mas, Benjamin Busam, Ales Leonardis, and Steven McDonagh. Cromo: Cross-modal learning for monocular depth estimation. In *Proceedings of the IEEE/CVF Conference on Computer Vision and Pattern Recognition*, pages 3937–3947, 2022.
- [48] Gu Wang, Fabian Manhardt, Federico Tombari, and Xiangyang Ji. Gdr-net: Geometry-guided direct regression network for monocular 6d object pose estimation. In *Proceedings of the IEEE/CVF Conference on Computer Vision and Pattern Recognition*, pages 16611–16621, 2021.
- [49] He Wang, Srinath Sridhar, Jingwei Huang, Julien Valentin, Shuran Song, and Leonidas J Guibas. Normalized object co-

ordinate space for category-level 6d object pose and size estimation. In *Proceedings of the IEEE Conference on Computer Vision and Pattern Recognition*, pages 2642–2651, 2019.

- [50] Pengyuan Wang, HyunJun Jung, Yitong Li, Siyuan Shen, Rahul Parthasarathy Srikanth, Lorenzo Garattoni, Sven Meier, Nassir Navab, and Benjamin Busam. Phocal: A multi-modal dataset for category-level object pose estimation with photometrically challenging objects. In *CVPR*, 2022.
- [51] Pengyuan Wang, Fabian Manhardt, Luca Minciullo, Lorenzo Garattoni, Sven Meier, Nassir Navab, and Benjamin Busam. Demograsp: Few-shot learning for robotic grasping with human demonstration. In *2021 IEEE/RSJ International Conference on Intelligent Robots and Systems (IROS)*, pages 5733–5740. IEEE, 2021.
- [52] Yu Xiang, Tanner Schmidt, Venkatraman Narayanan, and Dieter . Posecnn: A convolutional neural network for 6d object pose estimation in cluttered scenes. *Robotics: Science and Systems*, 2018.
- [53] Heng Yang, Jingnan Shi, and Luca Carlone. Teaser: Fast and certifiable point cloud registration. *IEEE Transactions on Robotics*, 37(2):314–333, 2020.
- [54] Guangyao Zhai, Yu Zheng, Ziwei Xu, Xin Kong, Yong Liu, Benjamin Busam, Yi Ren, Nassir Navab, and Zhengyou Zhang. Da2-dataset: Toward dexterity-aware dual-arm grasping. *IEEE Robotics and Automation Letters*, 7(4):8941–8948, 2022.

Supplementary Material for HouseCat6D Dataset



Figure 1. **Object Meshes from Symmetric and Partially Symmetric Shape Categories.** Glass (a), bottle (b), can (c) and tube (d) categories are the categories with distinctive symmetry axis. We align the y axis to the axis of symmetry. If one surface is larger in area than another side, the x -axis is aligned in perpendicular direction to it. All the objects are rendered in the same scale to highlight the size variance among the same category.

1. Object Meshes and Orientation

The HouseCat6D dataset features 194 highly diverse objects from 10 household object categories with different textures, sizes, and shapes. In this section, we show the meshes of the objects in each category and the descriptions of their orientation.

Glass HouseCat6D aligns the symmetry axis with the y axis for the (partially) symmetric objects. Glass objects in our dataset are fully symmetric around y axis in accordance with [3] who also align y axis and symmetry axis. The x and z axes serve as any orthogonal axes around the y axis as exemplified in Fig. 1 (a).

Bottle Unlike the glass objects, bottle objects in our dataset are sometimes not fully symmetric (i.e. frontal surface is wider than the side) as in Fig. 1 (b). In this case, we define the x axis perpendicular to the surface of larger area.

Can Similar to the bottle objects, can objects in our dataset sometimes are not fully symmetric (i.e. some cans are more square and one side is wider than the other side)

as shown in Fig. 1 (c). Like the bottle objects, we define the x axis perpendicular to the wider side.

Tube Tube objects in our dataset are partially symmetric in shape, such that one side is round at the end while flat on the other side as shown in Fig. 1 (d). As in the can and bottle category, we define the x axis perpendicular to the wider side.

Teapot In general, teapots have the shape of one (partially) symmetric body with a handle and tip where the liquid comes out. In our dataset, we use the y axis for the direction of the symmetric body and x axis for the direction from the handle to the tip as shown in Fig. 2 (a).

Cup For the cup category, we only use cups with handles that have the shape of one symmetric body with a handle. Thus, similar to the Teapot category, we align the y axis to the direction of the symmetric body and x with the direction from the handle to the other side of the body as shown in Fig. 2 (b).

Shoe Shoes, in general, have a long, flat and non-symmetric shape. For this category, we use only the right



Figure 2. **Object Meshes from (Partially) Symmetric Objects With a Handle.** Teapot (a) and cup (b) are the categories with objects that include a (partially) symmetric body with handle. We align the y axis with the symmetry axis of the body and the x axis with the direction from handle to the the other side of the body. All the objects are rendered in the same scale to highlight the size variance among the same category.



Figure 3. **Object Meshes from Flat Shape Categories.** Shoe (a), remote (b) and cutlery (c) are the categories with long, flat and non-symmetric shape. We oriented such shapes in a way that the y axis points in the direction of the upper side and x in the direction of the front side. All the objects are rendered in the same scale to highlight the size variance among the same category.



Figure 4. **Object Meshes for Box category.** Unlike the other categories, the sides of the box are rather defined by their texture. To allow networks to generalize in this category, we orient the meshes by their side length. We set y, x, z as direction of first, second and third longest side. All the objects are rendered in the same scale to highlight the size variance among the same category.

side of the slipper as illustrated in Fig. 3 (a). We oriented shoes such that their upper side points in the direction of the y axis and the front side points in the direction of the x axis.

Remote Remotes have relatively flat bodies with long and non-symmetric shapes, as shown in Fig. 3 (b). Similar to the shoe category, remotes are oriented such that their upper side points in the direction of the y axis, and the front side is oriented in the direction of the x axis.

Cutlery Although the texture of the reflective surface makes a clear distinction between the cutlery category to any other category, the shape itself shares similarity with shoe and remote category. It is flat, long, and non-symmetric (Fig. 3 (c)). Thus, it shares the same orientation scheme, the upper side is aligned with the y axis and the

front side points in x direction.

Box Unlike other categories, the sides of the box are defined by their texture. Even a human observer has to inspect the textures on multiple sides of a box to judge which side is the front or upper side *etc.* To make it easier for networks to generalize the orientation of boxes, we orient them by the length of the sides independent of their textures. We use y, x, z for the direction of the first, second, and third longest side as shown in Fig. 4.

2. External Tracking System Evaluation

As mentioned in Sec. 3.2 in the main paper, we evaluate our IR-based external tracking system ARTTRACK2 via a robotic arm. We use a KUKA LBR iiwa 7 R800 (KUKA Roboter GmbH, Augsburg, Germany), a 7 DoF robotic arm

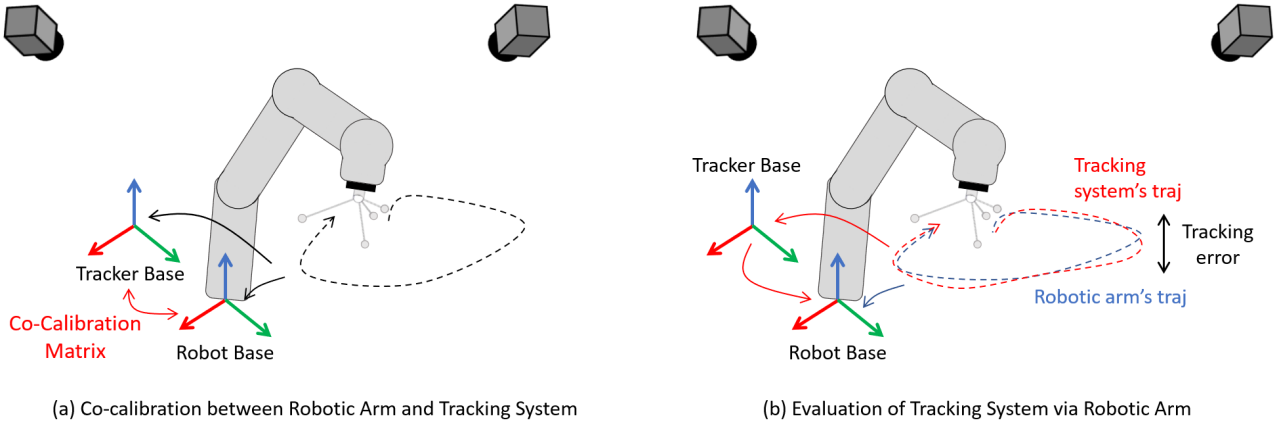


Figure 5. **Tracking System Evaluation.** We use a robotic arm to evaluate the quality of the tracking system. We first (a) co-calibrate the robot and the tracking system such that they share a common reference frame and then (b) run an example trajectory to calculate the difference between the trajectory obtained from the robot and the tracking system for error evaluation.

Approach	Train Set	3D ₂₅ / 3D ₅₀	Bottle	Box	Can	Cup	Remote	Teapot	Cutlery	Glass	Tube	Shoe
FS-Net [1]	Full	69.4 / 37.0	64.0 / 42.7	29.4 / 12.7	99.6 / 75.1	92.3 / 54.1	62.6 / 45.3	69.1 / 54.2	43.5 / 10.6	97.2 / 28.2	72.2 / 14.9	58.2 / 38.2
	Reduced	56.9 / 16.8	63.3 / 37.0	33.6 / 6.7	99.9 / 63.3	68.2 / 6.3	49.0 / 22.4	51.1 / 19.6	24.6 / 0.5	90.9 / 9.7	75.7 / 5.2	37.8 / 17.2

Table 1. **Pose Coverage Ablation.** Class-wise evaluation of 3D IoU (at 25%/ at 50%) for FS-Net [1] with the Full and a Reduced training split to mimic the limited pose coverage of PhoCal [4].

certified for industrial use to provide ± 0.1 mm positional reproducibility, as the device to produce the ground truth pose for the comparison. In this section, we describe the detailed steps for the evaluation.

2.1. Robot-Tracker Co-Calibration

The first step to evaluate the tracking system with a robot is to co-calibrate the base of the robot and the tracking system. For this, we attach the calibrated IR tracking body on the robotic End-Effector (EE) as shown in Fig. 5 (a). We then acquire one trajectory from two different coordinate bases, one from the Robot base and the other one from the Tracker base. Similar to hand-eye calibration, we extract the static transformation between the two trajectories using the method of Horn [2]. In this case, the static transformation matrix is the transformation between Tracker Base and Robot Base (marked red in Fig. 5 (a)).

2.2. Trajectory Error Evaluation

After co-calibration, we keep the tracking body on the robotic EE and make an evaluation trajectory that replicates the trajectory in one of the scenes. We repeat the trajectory twice, once with the robot stopping at every capturing position and once with the robot not stopping during the pose capture. The first trajectory serves as an evaluation for the tracking system accuracy in the static case, and the later trajectory serves as an evaluation in the dynamic case. As it is possible to obtain the pose of the tracking body from both,

robot and tracking system, in the same coordinate frame using the co-calibration matrix, the error of the tracking system is calculated as the pose difference between the pose from the robotic arm and the pose from the tracking system (Fig. 5 (b)). We measure an error of 0.67 mm / 0.12° in the static case and 0.92 mm / 0.16° in the dynamic case.

3. Ablation Study

We train FS-Net [1] on data of our dataset HouseCat6D but with a similar data distribution as in PhoCal [4] in terms of reduced number of scenes, trajectories and pose coverage. Tab. 1 summarizes the results from the reduced dataset against the result from the full dataset. The ablation confirms our motivation for the need to provide an extensive 6D object pose dataset with comprehensive pose coverage. Objects with a certain degree of overall symmetry in shape (like Box, Can or Glass) only suffer to a relatively small extent from the reduced pose coverage during training. In contrast, objects with a distinct non-symmetric feature, e.g. the handle of a cup or teapot, show a significant drop in accuracy, especially in the more constrained 3D50.

References

- [1] Wei Chen, Xi Jia, Hyung Jin Chang, Jinming Duan, Linlin Shen, and Ales Leonardis. Fs-net: Fast shape-based network for category-level 6d object pose estimation with decoupled rotation mechanism. In *Proceedings of the IEEE/CVF Conference on Computer Vision and Pattern Recognition (CVPR)*, pages 1581–1590, June 2021. 3
- [2] Berthold Horn, Hugh Hilden, and Shahriar Negahdaripour. Closed-form solution of absolute orientation using orthonormal matrices. *Journal of the Optical Society of America A*, 5:1127–1135, 07 1988. 3
- [3] He Wang, Srinath Sridhar, Jingwei Huang, Julien Valentin, Shuran Song, and Leonidas J Guibas. Normalized object coordinate space for category-level 6d object pose and size estimation. In *Proceedings of the IEEE Conference on Computer Vision and Pattern Recognition*, pages 2642–2651, 2019. 1
- [4] Pengyuan Wang, HyunJun Jung, Yitong Li, Siyuan Shen, Rahul Parthasarathy Srikanth, Lorenzo Garattoni, Sven Meier, Nassir Navab, and Benjamin Busam. Phocal: A multi-modal dataset for category-level object pose estimation with photo-metrically challenging objects. In *CVPR*, 2022. 3